First-principles study of substitutional magnesium and zinc in hydroxyapatite and octacalcium phosphate

AUTHOR(S):

Matsunaga, Katsuyuki

CITATION:

Matsunaga, Katsuyuki. First-principles study of substitutional magnesium and zinc in hydroxyapatite and octacalcium phosphate. JOURNAL OF CHEMICAL PHYSICS 2008, 128(24): 245101.

ISSUE DATE:

2008-06-28

URL:

http://hdl.handle.net/2433/84601

THE JOURNAL OF CHEMICAL PHYSICS **128**, 245101 (2008)

First-principles study of substitutional magnesium and zinc in hydroxyapatite and octacalcium phosphate

Katsuyuki Matsunaga[a)]
Department of Materials Science and Engineering, Kyoto University, Yoshida-Honmachi, Sakyo, Kyoto 606-8501, Japan and Nanostructure Research Laboratory, Japan Fine Ceramics Center, 2-4-1, Mutsuno, Atsuta, Nagoya, 456-8587 Japan

(Received 17 March 2008; accepted 14 May 2008; published online 24 June 2008)

First-principles calculations are performed for Mg^{2+} and Zn^{2+} substitution in hydroxyapatite (HAp) and octacalcium phosphate (OCP), because the foreign ions are known to play an important role for bone formation. In order to study their possible location in the system of HAp in contact with the aqueous solution, OCP is considered as a structural model of the transition region between HAp and the solution. It is found that, when the foreign ions substitute for Ca sites, the surrounding oxygen ions undergo considerable inward relaxation, due to their smaller ionic sizes than Ca^{2+}, which results in the smaller coordination numbers with oxygen as compared with those of Ca in bulk HAp and OCP. From the calculated defect formation energies, it is likely that the substitutional foreign ions are quite difficult to dissolve into HAp whereas can be more easily incorporated in OCP. In particular, Zn^{2+} can more favorably substitute for the specific Ca site of OCP, as compared to Mg^{2+}, which is attributed with covalent bond formation between Zn and the surrounding oxygen ions. It is thus considered that zinc may play its role to promote bone formation by being incorporated into the transition region between HAp and the surrounding solution. © *2008 American Institute of Physics*. [DOI: 10.1063/1.2940337]

I. INTRODUCTION

In normal bone remodeling processes, successive bone resorption and formation take place with the aid of osteoclast and osteoblast activity. Imbalance between bone resorption and formation results in osteoporosis, which is a bone disease characterized by decreased bone mass and density. Since hard tissues such as bone and tooth enamel contain hydroxyapatite [$Ca_{10}(PO_4)_6(OH)_2$ (HAp)] as inorganic components, it is essential to clarify physical and chemical properties of biological HAp and to obtain a fundamental understanding of the bone mineralization processes.

It is known that hard tissues in human bodies contain a variety of trace elements, which likely play important biological roles. Typical trace elements in bones and tooth enamels are ~4–8 wt % of carbonate (CO_3^{2-}), ~0.4–0.9 wt % of sodium and magnesium, and approximately less than 0.1 wt % of potassium, fluoride, and chloride.[1] Among trace elements involved in bones and the surrounding aqueous solutions (body fluids), magnesium and zinc ions are expected to have a significant effect on bone mineralization. The content of Mg^{2+} in biological apatites is basically larger than that of Zn^{2+}, and the trace elements are considered to be uptaken and/or released by bone-mineral components during the bone remodeling process. Regarding the trace-element effects on bone formation, it was reported that the Mg^{2+} deficiency gives rise to decreased bone mass, due to decreased osteoblasts and increased osteoclasts.[2] While it is known that Zn^{2+} addition can stimulate osteoblast activity and thus promote bone formation.[3] Hayakawa *et al.* also reported that Zn-doped HAp particles exhibit selective protein adsorption.[4] It is expected, therefore, that Mg and Zn dopants may play a potential role for adsorption of proteins and cells on biological apatites. In addition to their biological effect, these ions are known to inhibit crystallization and growth of HAp, which indicates that they also affect formation, crystal sizes, and morphology of the HAp minerals in bone and tooth.[5–8]

In order to clarify the effects of Mg^{2+} and Zn^{2+} on bone formation in more detail, it is necessary to investigate their location and chemical environments in the system of HAp and its surrounding solution at the atomic and electronic levels. In particular, the role of the trace elements for bone formation may be different depending on their location. When the situation that HAp is in contact with an aqueous solution is considered,[9,10] it can be simply imagined that there are three main possibilities of the locations of the trace elements; (1) substitution for Ca^{2+} in the HAp lattice, (2) the incorporation in a transition region between HAp and the solution, and (3) being loosely bound at HAp surfaces or in the solution. In the first case, it is considered that the trace elements cannot directly affect the bone formation but could play its role only when the ions are released by dissolution of HAp crystals. The second case could promote adsorption of osteoblast cells on the transition region and could directly stimulate the activity of the adsorbed cells. Since apatite crystals in mineralized bones are always thin and platelet with a thickness of about 4 nm,[1] many atoms in the crystals may be considered to be located in the transition region. Therefore, it is inevitably important to investigate impurity

a)Author to whom correspondence should be addressed. Electronic mail: k.matsunaga@materials.mbox.media.kyoto-u.ac.jp.

location in the transition region as well as in HAp. However, the transition region may have a low-crystalline state or a hydrated state of calcium phosphate, and its detailed structure has not been characterized because that phase may be metastable.[11–13] In this regard, Brown *et al.* proposed that the structure of the transition region is similar to the structure of octacalcium phosphate [$Ca_8H_2(PO_4)_6 \cdot 5H_2O$ (OCP)], which has ionic arrangements of Ca^{2+} and PO_4^{3-} similar to HAp and also contains H_2O molecules (details will be shown later).[14] Santos *et al.* and Cazalbou *et al.* also suggested the presence of the metastable hydrated layer containing HPO_4^{2-} and structural water molecules on the HAp surface, which resembles the OCP structure.[12,13] In the third case, the ions may directly act on osteoblast cells to promote protein synthesis and enzyme activity. In order to understand the bone formation mechanism by the trace elements, therefore, it is essential to reveal the possible locations in the system containing HAp and its surrounding solution.

Recently, first-principles calculations have proved to be effective to investigate atomic and electronic structures of point defects even in complicated metal oxides such as apatite-based materials. By analyzing total energies of computational models, it is also feasible not only to reveal characteristic atomic coordinates but also to evaluate defect energetics quantitatively.[15,16] Regarding Mg^{2+} and Zn^{2+} ions in calcium phosphates, Terra *et al.* employed the embedded cluster model method to study electronic structures of Zn^{2+} in HAp.[17] Yin *et al.* carried out first-principles calculations of Mg^{2+} and Zn^{2+} dopants in tricalcium phosphate (TCP) using cluster models, and discussed the bioactivity of the TCP materials from the structural characteristics around the dopants.[18] More recently, Ma and Ellis calculated Zn substitution on the HAp (0001) surface, using the surface slab models, and evaluated adsorption energies at Ca sites around the surface.[19] Although these studies provided detailed atomic structures around the dopants, they did not evaluate thermodynamic stability of Mg^{2+} and Zn^{2+} in the apatite-related materials.

In this study, first-principles band-structure calculations are performed for Mg^{2+} and Zn^{2+} in HAp. In order to investigate a possibility of their incorporation into the HAp-solution transition region, OCP is used as a structural model, and substitution of Mg^{2+} and Zn^{2+} for Ca in OCP is also calculated. Theoretical formation energies of the substitutional defects are evaluated from total energies of supercells, together with chemical potentials determined under chemical equilibrium between HAp and its saturated aqueous solution. The predicted locations of the trace elements are discussed in connection with their role in the bone formation process.

II. COMPUTATIONAL METHOD

A. Electronic structure calculation

First-principles electronic structure calculations are performed based on the projector augmented wave method, implemented in VASP.[20–22] The generalized gradient approximation (GGA) is used for the exchange-correlation potential, and the GGA functional proposed by Perdew *et al.* is employed.[23] A plane-wave cutoff energy (E_{cut}) of 500 eV is used throughout the present study. Based on forces on atoms calculated, all atoms in unit cells and supercells are allowed to relax until their forces converge to less than 0.05 eV/Å.

In this study, substitutional Mg^{2+} and Zn^{2+} for Ca^{2+} in HAp and OCP are calculated. Since these are divalent cations, additional charge compensating defects do not need to be considered for the ion substitutions. For HAp, the hexagonal structure (space group $P6_3/m$) having 44 atoms is used.[24] It is noted that the P atom is surrounded by four O atoms with a bond length of 0.156 nm, two kinds of Ca sites, Ca-1 and Ca-2, are present, and the OH^- ions are not in the positions related by the mirror planes at $z=1/4$ and $3/4$. The Ca-1 ions are sixfold coordinated by oxygen ions at the vertices of PO_4 tetrahedra, with a Ca–O bond length of about 0.24 nm (see Table I). Since Ca-1 ions form columns along the c axis, therefore, they are sometimes referred to as columnar Ca. The Ca-2 ions are also surrounded by six oxygen ions, and form two Ca triangles rotated by 60° about the OH^- columns parallel to the c axis. Further details of the hexagonal structure were also described in Refs. 24 and 25. The unit-cell structure of the hexagonal phase was already optimized in the same first-principles manner with the present study,[15] which is used to generate HAp supercells for the defect calculations.

TABLE I. The calculated interatomic distances and coordination numbers from Ca and P to their neighboring atoms in bulk HAp and OCP.

	Distances (nm) (atomic species; coordination number)	
Atomic site	First NN	Second NN
	HAp	
Ca-1	0.244(O;3), 0.248(O;3)	0.280(O;3)
Ca-2	0.236(O;3), 0.240(O;1), 0.248(O;1), 0.252(O;1)	0.269(H;1),0.281(O;1)
P	0.156(O;4)	
	OCP	
Ca-1	0.241(O;1), 0.246(O;4), 0.251(O;1), 0.267(O;1)	0.279(O;1)
Ca-2	0.238(O;3), 0.241(O;1), 0.250(O;2), 0.263(O;1)	0.301(O;1)
Ca-3	0.228(O;1), 0.239(O;1), 0.247(O;3), 0.256(O;1)	0.287(O;1)
Ca-4	0.234(O;1), 0.238(O;2), 0.246(O;1), 0.254(O;2), 0.261(O;1)	0.295(H;1)
Ca-5	0.234(O;1), 0.237(O;2), 0.242(O;1), 0.246(O;1), 0.249(O;1)	0.275(H;1)
Ca-6	0.227(O;3), 0.237(O;1), 0.251(O;1), 0.271(O;1)	0.287(O;1)
Ca-7	0.231(O;1), 0.237(O;2), 0.246(O;1), 0.250(O;2), 0.258(O;1)	0.279(H;1)
Ca-8	0.238(O;1), 0.240(O;2), 0.242(O;2), 0.267(O;1)	0.308(O;1), 0.311(P;1)
P-1	0.156(O;4)	
P-2	0.156(O;4)	
P-3	0.156(O;4)	
P-4	0.156(O;4)	
P-5	0.154(O;3), 0.163(O;1)	
P-6	0.155(O;3), 0.160(O;1)	

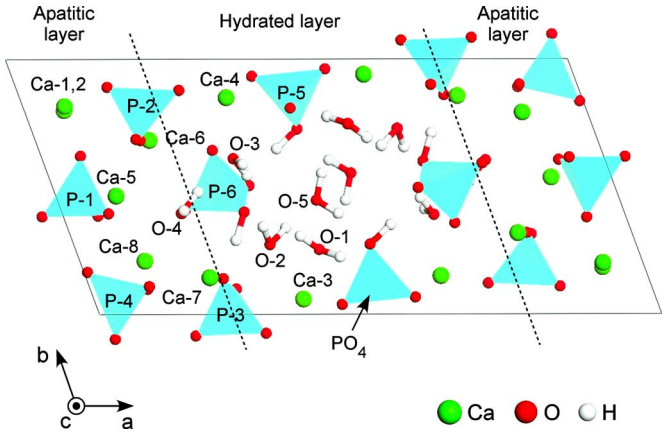

FIG. 1. (Color online) Crystal structure of OCP viewed along the c axis. The PO_4^{3-} groups are represented by the tetrahedra.

Figure 1 displays the unit-cell structure of OCP viewed along the c axis. The crystal structure is triclinic with a space group of $P\bar{1}$ and exhibits the much longer a-axis dimension than the b axis.[14,26] There are eight kinds of Ca sites and six kinds of P sites, and the P atoms are surrounded by four oxygen atoms to form PO_4 tetrahedra. According to the notations by Mathew *et al.*,[26] PO_4 tetrahedra centered at P-5 and P-6 are in the form of HPO_4 groups by hydrogen attachment. Except for oxygen atoms bonded to the P atoms, there are five kinds of crystallographically independent O atoms (O-1 to O-5) forming H_2O molecules. It is noted that O-3 is statistically disordered and two kinds of O-3 positions, O-3a and O-3b, were designated by Mathew *et al.*[26] Many of the H_2O molecules are coordinated to adjacent Ca atoms. O-1 is coordinated to Ca-3, O-2 to two Ca atoms of Ca-3 and Ca-7, and O-3 to Ca-4. O-4 is also bonded to Ca-5 and Ca-7, whereas O-5 is not coordinated to Ca atoms. Due to the center of inversion at $(1/2,1/2,1/2)$, the total number of atoms in the unit cell is 110.

As shown by Brown *et al.*,[14] the OCP structure is closely related to HAp. In OCP, the atomic arrangement of Ca and PO_4 in the region of $x=0-1/4$ and $x=3/4-1$ is similar to that of HAp, and therefore is referred to as the "apatitic layer." Due to the similarity to HAp, OCP is considered as a precursor of HAp in *in vitro* and in pathological calcification.[11] It is noted, however, that the local atomic coordinates are more distorted and lower symmetric than those in HAp. In contrast, the remaining region containing the water molecules is called as the hydrated layer, and the composition in this layer $(Ca_4(HPO_4)_4\cdot 10H_2O)$ is close to that of dicalcium phosphate dehydrate $[Ca(HPO_4)\cdot 2H_2O]$.[27] The apatitic and hydrated layers are alternately stacked along the a axis in the OCP structure.

The OCP unit cell is calculated on the Monkhorst–Pack k-point mesh of $1\times 2\times 3$ (three irreducible k points).[28] As stated above, since O-3 is disordered,[26] two kinds of the OCP unit cells comprising O-3a and O-3b are calculated, so that a total energy of the unit cell containing O-3b is found to be by 0.35 eV smaller than that of the O-3a case. Accordingly, computed results based on the unit cell with O-3b will be shown hereafter. The optimized unit-cell parameters are $a=2.00$ nm, $b=0.97$ nm, $c=0.69$ nm, $\alpha=90.35°$, $\beta=93.21°$, and $\gamma=110.14°$, which reproduce experimental data within an accuracy of 1.7%.[26]

The calculated distances from Ca and P to the first and second nearest neighbor (NN) atoms in HAp and OCP are summarized in Table I. In HAp, the Ca-1 and Ca-2 sites are considered to be sixfold coordinated by oxygen. However, the extended coordination numbers of Ca within the second NN coordination shell (9 for Ca-1 and 7 for Ca-2) are sometimes used to discriminate the difference in atomic coordination of Ca-1 and Ca-2.[25] As compared to the HAp case, the Ca–O lengths in OCP exhibit a wide range of variation from 0.23 to 0.28 nm, but it can be roughly said from Table I that the coordination numbers of Ca to O are 6 or 7. In contrast, the P–O lengths in OCP are similar to those in HAp (about 0.156 nm), and all the P atoms are fourfold coordinated by oxygen. However, a H atom attaches to an O atom of the PO_4 tetrahedra centered at P-5 and P-6, and then the P–O bond with the hydrogen attachment exhibits a longer bond length (about 0.16 nm) than the other three P–O bonds.

Based on the optimized unit-cell structures of HAp and OCP, supercells for the defect calculations are generated. In the HAp case, the hexagonal unit cell is doubled in all directions, so that the HAp supercell comprises 352 atoms. While the OCP unit cell is doubled only along the c axis, and the total atomic number of the resultant OCP is 220 atoms. For the supercell calculations, Brillouin zone integrations are performed only at Γ point because of the rather large supercells. One of Ca atoms is replaced by Mg or Zn, and the substitution at all the inequivalent Ca sites is individually calculated in both the HAp and OCP cases. All atoms in the defective supercells are allowed to relax in the manner described above, but the cell shape and cell dimensions are kept constant during the structural optimization. This corresponds to the ion substitution in HAp and OCP in the dilute state. If a large amount of the substitutional defects are accommodated in the crystals, defect-defect interactions, statistic defect configurations of defect species, and the associated variations in the lattice parameters of HAp may be taken into account. As a first step, however, it is beneficial to study formation energies of the isolated substitutional defects based on the dilute approximation, in order to reveal fundamental solubility of Mg and Zn in HAp and OCP.

In order to check the computational accuracy in the present supercell calculations, test calculations using two irreducible k points are carried out for the OCP supercells with/without Zn substitution. It is confirmed that the total energy convergence is less than 1.0 meV/atom, which results in a difference in defect formation energy of less than 0.01 eV.

B. Defect formation energy

Defect formation energies (ΔH_f) are evaluated from total energies (E_T) of the perfect and defective supercells. When a divalent foreign ion M^{2+} (M=Mg or Zn) substitutes for Ca^{2+} in HAp or OCP, ΔH_f can be written as

$$\Delta H_f = E_T(\text{defective}) - E_T(\text{perfect}) + \bar{\mu}_{Ca^{2+}} - \bar{\mu}_{M^{2+}}. \quad (1)$$

Here $\bar{\mu}_{Ca^{2+}}$ and $\bar{\mu}_{M^{2+}}$ indicate electrochemical potentials of Ca^{2+} and M^{2+}, which are determined from chemical equilibrium of interest. In this study, it is assumed that HAp and OCP crystals equilibrate with an aqueous solution that is saturated with respect to HAp and contains particular amount of M^{2+} ions. Since the electrochemical potentials of a constituent ionic species in the solid and liquid phases are equal to each other in the chemical equilibrium, $\bar{\mu}_{Ca^{2+}}$ and $\bar{\mu}_{M^{2+}}$ can be determined from those for the ions dissolving in the aqueous solution to evaluate the defect formation energies.

It is noted that the electrochemical potential for an ionic species M^{2+} in a solution is expressed in terms of a standard chemical potential $\mu^{\circ}_{M^{2+}}$, an activity ($a_{M^{2+}}$), and an inner potential of the solution ϕ_{aq} as[29,30]

$$\bar{\mu}_{M^{2+},aq} = \mu^{\circ}_{M^{2+},aq} + k_B T \ln a_{M^{2+}} + 2\phi_{aq}, \quad (2)$$

where k_B is the Boltzmann constant and T is the temperature. The temperature of 298 K is used throughout the present study. Substituting Eq. (2) into Eq. (1) gives rise to the defect formation energy as

$$\Delta H_f = E_T(\text{defective}) - E_T(\text{perfect}) + \mu^{\circ}_{Ca^{2+},aq} - \mu^{\circ}_{M^{2+},aq} + k_B T \ln(a_{Ca^{2+}}/a_{M^{2+}}). \quad (3)$$

The standard chemical potential terms $\mu^{\circ}_{Ca^{2+},aq}$ and $\mu^{\circ}_{M^{2+},aq}$ are obtained by invoking chemical reactions to form the ionic species in aqueous solution in the standard state. For Ca^{2+}, the following reaction,

$$Ca(s) \rightarrow Ca^{2+}(aq, a_{Ca^{2+}} = 1) + 2e^-, \quad (4)$$

is considered, and then $\mu^{\circ}_{Ca^{2+},aq}$ is expressed by using the Gibbs energy change for the reaction $\Delta G^{\circ}_f(Ca^{2+},aq)$ as

$$\mu^{\circ}_{Ca^{2+},aq} = \Delta G^{\circ}_f(Ca^{2+},aq) + \mu^{\circ}_{Ca,s} - 2\mu^{\circ}_{e^-,aq}. \quad (5)$$

Likewise, $\mu^{\circ}_{M^{2+},aq}$ can be obtained, and thus the chemical potential difference in Eq. (3) is given by

$$\mu^{\circ}_{Ca^{2+},aq} - \mu^{\circ}_{M^{2+},aq} = \Delta G^{\circ}_f(Ca^{2+},aq) - \Delta G^{\circ}_f(M^{2+},aq) + \mu^{\circ}_{Ca,s} - \mu^{\circ}_{M,s}. \quad (6)$$

The last two terms of the right-hand side of Eq. (6) correspond to the chemical potentials of pure metallic Ca and M. In this study, total energies per atoms for bcc Ca and hcp Mg and Zn are separately calculated in the first-principles manner and are used for $\mu^{\circ}_{Ca,s}$ and $\mu^{\circ}_{M,s}$. In contrast, in order to obtain $\Delta G^{\circ}_f(Ca^{2+},aq)$ and $\Delta G^{\circ}_f(M^{2+},aq)$ by the first-principles method, it is necessary to calculate the ions dissolving in the aqueous solution. However, such calculations are not always easy to perform because of the complexity of the hydrated atomic structures in an aqueous solution. Since the standard Gibbs formation energies for ions in aqueous solution (at 298 K) can be found in the thermodynamic table,[31] therefore, the experimental data are used for the quantities in this case.

The ionic activities of $a_{Ca^{2+}}$ and $a_{M^{2+}}$ in Eq. (3) comprise activity coefficients γ and concentrations of the ionic species ($[Ca^{2+}]$ and $[M^{2+}]$) in the solution (e.g., $a_{M^{2+}} = \gamma_{M^{2+}}[M^{2+}]$). In order to evaluate the activity of the ions in the solution, the following situations are assumed in this study: (a) the activity coefficients are assumed to be unity because the HAp-saturated solution is basically a dilute one due to the small solubility product of HAp,[25] (b) the M^{2+} ions of particular concentrations are introduced into the solution by addition of MA_2 compounds (e.g., $A^- = NO_3^-$), as encountered in the previous experiments,[6,7,32] (c) the solution pH is adjusted by adding acid HX in the low pH range and base BOH in the high pH range,[33] and (d) the A^-, B^+, and X^- ions are indifferent ions to dissolution equilibrium of HAp. As a result, in the low pH range, the charge neutrality condition of the solution can be written as

$$2[Ca^{2+}] + 2[M^{2+}] + [H^+] = [A^-] + [X^-] + [OH^-] + 3[PO_4^{3-}] + 2[HPO_4^{2-}] + [H_2PO_4^-], \quad (7)$$

where

$$2[M^{2+}] = [A^-] \quad (8)$$

and

$$[H^+] = [X^-]. \quad (9)$$

It is noted here that the phosphate ions have three different protonated forms, HPO_4^{2-}, $H_2PO_4^-$, and H_3PO_4 in the solution, depending on the solution pH. In a similar way, the charge neutrality in the high pH range is described as

$$2[Ca^{2+}] + 2[M^{2+}] + [H^+] + [B^+] = [A^-] + [OH^-] + 3[PO_4^{3-}] + 2[HPO_4^{2-}] + [H_2PO_4^-], \quad (10)$$

where the following relation is imposed, together with Eq. (8);

$$[B^+] = [OH^-]. \quad (11)$$

In addition to the above charge neutrality requirements, the ionic product of water, the solubility product of HAp,[34] and the three different acid dissociation constants for phosphate ions ($HPO_4^{2-} = PO_4^{3-} + H^+$, $H_2PO_4^- = HPO_4^{2-} + H^+$, and $H_3PO_4 = H_2PO_4^- + H^+$) are used to calculate the ionic concentration of Ca^{2+} as a function of the solution pH. More details can also be found elsewhere.[35] Figure 2 displays the calculated pH dependence of Ca^{2+} concentration in the HAp-saturated aqueous solution. It can be seen that the Ca^{2+} concentration tends to increase with decreasing pH.[33] When the pH condition and the $[M^{2+}]$ value of the solution are given, therefore, the defect formation energy for the ion substitution can be obtained as a function of pH.

III. RESULTS AND DISCUSSION

A. Electronic structure of bulk HAp and OCP

Before going to ion substitution in HAp and OCP, electronic structures of perfect HAp and OCP lattices are investigated. Figure 3 shows total densities of states (DOS) for the valence bands (VBs) of HAp and OCP. As found in the pre-

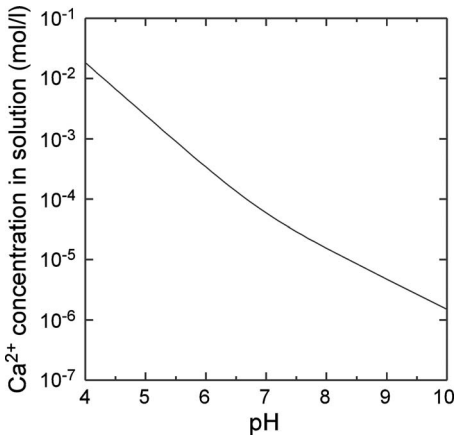

FIG. 2. pH dependence of Ca^{2+} concentration in the aqueous solution saturated with respect to HAp.

vious reports, the VB structure of HAp was described in detail,[15,36,37] and thus a number of characteristics in the VB are briefly summarized here. The lower VB of HAp is composed of O-2*s* and Ca-3*p* orbitals, while O-2*p* orbitals are a main component of the upper VB. The conduction band comprises Ca-3*d* and 4*s* orbitals, and the theoretical band gap of 5.3 eV agrees with the previous theoretical data.[36,37] It is also noted that the upper VB exhibits four prominent peaks, which arise mainly from strong admixture between P-3*sp* and O-2*sp* orbitals in the energy range of −8 to −4 eV and from overlap of Ca-3*d*4*s* and O-2*p* orbitals in the range of −4–0 eV.[15]

The band gap for OCP is calculated to be 4.9 eV, which is slightly smaller than that of HAp, and the overall DOS

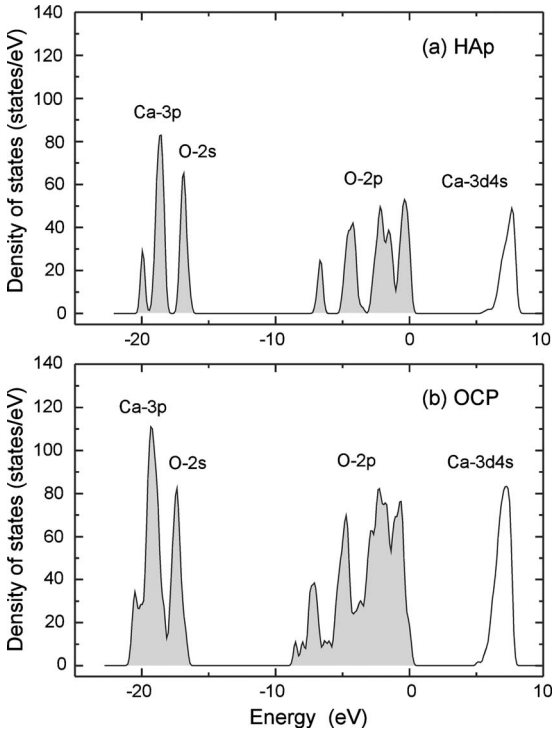

FIG. 3. Total DOS curves for perfect HAp and OCP. The shaded areas indicate the upper and lower VBs occupied by electrons. The VB maximum is set at 0 eV.

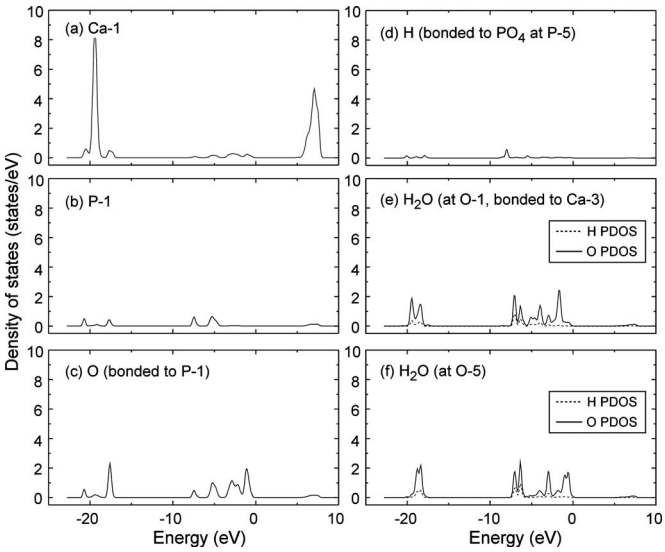

FIG. 4. Atom-projected partial DOS curves for constituent atoms in OCP.

feature is similar to that for HAp. The only difference in DOS from HAp is that small DOS components are observed between two neighboring peaks of the four prominent ones in the upper VB. This is mainly because OCP contains HPO_4 groups and H_2O molecules in its unit-cell structure, which are not found in HAp. In fact, it can be seen from the partial DOS curves in Fig. 4 that the energy levels originating from the proton of HPO_4 (centered at P-5) and the H_2O molecules also lie in the same energy range with O-2*p* components from PO_4 groups in the apatitic layer. Such complexity of the unit-cell structure of OCP results in the slight difference in DOS between HAp and OCP.

B. Atomic structures of substitutional magnesium and zinc in HAp

In order to investigate structural characteristics around Mg^{2+} and Zn^{2+} in HAp, the calculated distances from the substitutional cations to the neighboring atoms are investigated.[38] The coordination numbers of Mg^{2+} to oxygen within the first NN shell are 6 at both the Ca-1 and Ca-2 sites, as is the case in perfect HAp (see Table I). However, the bond distances from Mg^{2+} to the first NN oxygen atoms are by about 8.5% on average smaller than the nearest neighboring Ca–O distances in the perfect lattice. This can be understood from the much smaller ionic radius of Mg^{2+} (0.072 nm) than that of Ca^{2+} (0.100 nm) in the sixfold coordination.[39].

Since Zn^{2+} is also much smaller in size (0.074 nm) than Ca^{2+},[39] the similar inward relaxation of the first NN oxygen atoms can be found for Zn^{2+} substitution for Ca-1, whereas the local atomic coordination of Zn^{2+} at the Ca-2 site is quite different from the Ca-1 case. The interatomic distance from Zn^{2+} at the Ca-2 site to first NN oxygen is by about 13% shorter than that in the perfect lattice, and the resultant coordination number within the first NN shell becomes 4. In fact, it can be seen in the relaxed geometry of Fig. 5 that the OH^- group adjacent to Zn^{2+} is significantly displaced from the *c* axis toward Zn^{2+}, where the Zn–OH distance is 0.205 nm. Since Zn atoms prefer to have fourfold coordination with

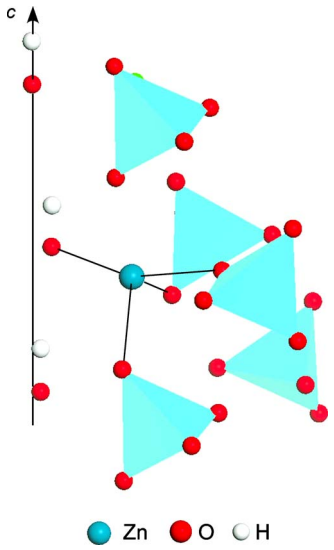

FIG. 5. (Color online) Optimized atomic structure around Zn^{2+} substituting for Ca-2 in HAp. The first NN oxygen atoms in the fourfold coordination state are shown by being connected with Zn^{2+} by the thin solid lines. The surrounding tetrahedra represent PO_4^{3-} groups.

oxygen as found in bulk ZnO, it is thought that the ZnO_4 tetrahedral configuration can also be formed depending on the substitutional sites in HAp. It seems likely that structural constraint at the Ca-2 site is less than that at Ca-1, due to the presence of the relatively mobile OH^- group at the adjacent site.

Figures 6(a) and 6(b) display partial densities of states (PDOSs) of Mg^{2+} and Zn^{2+} in HAp. In this case, the PDOS curves of the first NN oxygen atoms are also plotted. As stated in Fig. 1, the upper VB in HAp is mainly composed of O-2*p*, and the Mg-3*sp* orbitals only slightly contribute to the upper VB. This indicates a typical ionic character of bonding between Mg and the first NN oxygen in HAp. In Fig. 6(b), the Zn-3*d* band is located at around −5 eV, and also the Zn-4*sp* orbitals more contribute to the upper VB, as compared to Mg-3*sp* in Fig. 6(a). Although Zn-3*d* orbitals are fully occupied by electrons [electronic configuration of $3d^{10}$], the originally unoccupied Zn-4*sp* orbitals overlap with O-2*p* orbitals in a bonding manner, which results in covalent bond formation of Zn–O. This can also be observed in the contour maps of the charge densities for Mg^{2+} and Zn^{2+} at the Ca-2 site shown in Fig. 7. In the case of Mg^{2+} [Fig. 7(a)], the electron densities of Mg^{2+} and the adjacent oxygen of the OH^- group exhibit slight overlap, which is quite similar to the electron densities around ionically bonded Ca–O. However, more electrons are accumulated between Zn^{2+} and O^{2-} in Fig. 7(b), as compared with the Mg^{2+} case. It can be thought, therefore, that Zn^{2+} at Ca-2 tends to have the decreased coordination number of 4 so as to make the strong covalent bonds with O in the tetrahedral configuration.

C. Atomic structures of magnesium and zinc substitution in OCP

Atomic coordination structures for Mg^{2+} and Zn^{2+} in OCP are also investigated.[38] As also stated in Table I, the Ca–O bond lengths in perfect OCP exhibit the wide variation of 0.23–0.28 nm. This is also the cases for Mg^{2+} and Zn^{2+} substitution. In order to define the first NN coordination shell for the substitutional defects, therefore, the radius of a 15% larger value (0.24 nm) of the interatomic distances of Mg–O and Zn–O in bulk MgO and ZnO (about 0.21 nm) is used.[38]

The Mg–O distances in OCP vary in the range of 0.20–0.24 nm, which is by about 15% smaller than the Ca–O lengths in bulk OCP. In addition, the coordination

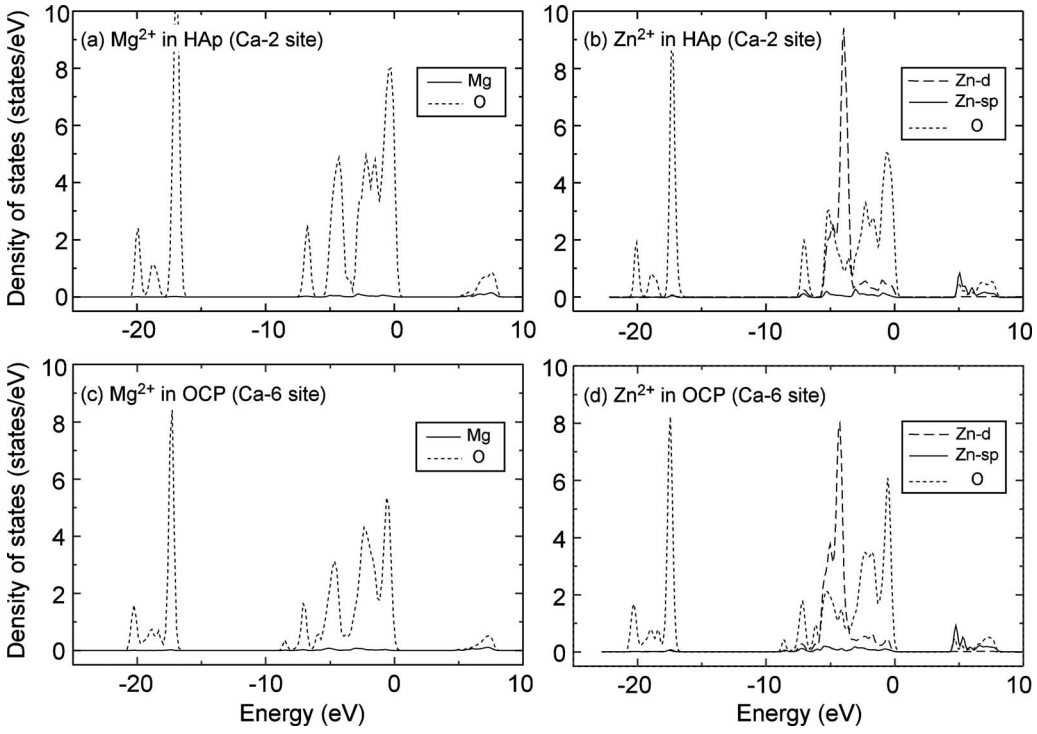

FIG. 6. Atom-projected PDOS curves for Mg^{2+} and Zn^{2+} in HAp and OCP. In the figures, the PDOS profiles of the first NN oxygen atoms are also depicted.

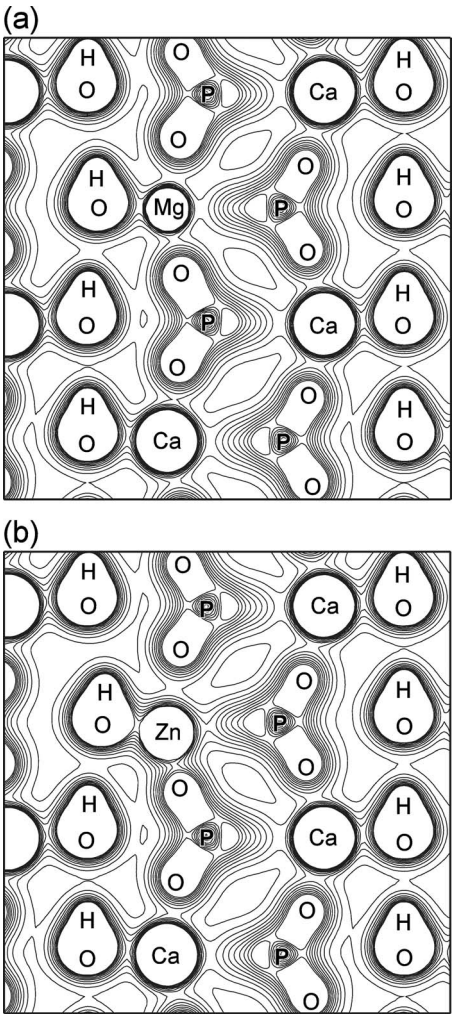

FIG. 7. Contour maps of electron densities around Mg^{2+} and Zn^{2+} at the Ca-2 site of HAp. The contour lines are drawn with an interval of 0.05 from 0.0 to 0.5 electrons/Å^3.

numbers of Ca to the first NN O atoms are 6 or 7 in bulk OCP, whereas the Mg^{2+} ions at the Ca-2, Ca-3, Ca-4, Ca-6, and Ca-8 sites in OCP are fivefold coordinated by the first NN O atoms. The tendency of the decreased coordination numbers of Mg^{2+} is attributed to its small ionic radius and interactions between the surrounding oxygen ions. It can be imagined that, when the small-sized cation is incorporated at the large-sized Ca^{2+} site, the surrounding O^{2-} ions tend to move toward the cation due to the size difference. Simultaneously, however, the negatively charged O^{2-} ions come close to one another around Mg^{2+}, which induces considerable electrostatic repulsion between the O^{2-} ions. In order to reduce energy penalty of the O^{2-}–O^{2-} interactions, a number of O^{2-} ions move away from the cation site, so that the coordination numbers of Mg^{2+} with O^{2-} in OCP tend to decrease depending on the substitutional sites. Such considerable atomic relaxation may be allowed due to the low symmetry of the OCP structure.

In the case of Zn^{2+} in OCP, the similar decreases in the bond lengths and the coordination numbers with first NN oxygen can be observed.[38] It should be noted, however, that the coordination numbers of Zn^{2+} in OCP are 4 or 5, depending on the atomic sites, which are smaller even compared

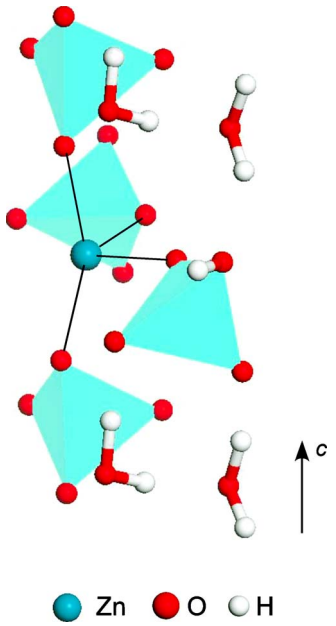

FIG. 8. (Color online) Optimized atomic structure of Zn^{2+} at the Ca-6 site in OCP. The first NN oxygen atoms in the fourfold coordination state are shown by being connected with Zn^{2+} by the thin solid lines. The surrounding tetrahedra indicate PO_4^{3-} groups.

with those of Mg^{2+} (the fivefold or sixfold coordination). As an example, the optimized atomic structure of Zn^{2+} at Ca-6 is displayed in Fig. 8. Since Zn in bulk ZnO has a smaller coordination number of 4 with oxygen than that of Mg in bulk MgO (sixfold coordinated), it can be expected that Zn^{2+} in OCP also tends to favor the fourfold coordination. Such a tendency can also be seen in the case of Zn^{2+} at the Ca-2 site of HAp (Fig. 5).

The PDOS curves of Mg^{2+} and Zn^{2+} at the Ca-6 sites are plotted in Figs. 6(c) and 6(d). These results are quite similar to those in HAp [Figs. 6(a) and 6(b)], where the Zn-4*sp* orbital components more contribute to the upper VB comprising O-2*p* orbitals, as compared to the Mg^{2+} case. It can be said, therefore, that the Zn^{2+} ion substituting for Ca is stabilized by covalent interactions with the surrounding O atoms at the expense of the decreased coordination numbers.

D. Thermodynamic stability of substitutional magnesium and zinc

As shown above, substituted Mg^{2+} and Zn^{2+} ions for Ca in HAp and OCP tend to have the smaller coordination numbers with oxygen, and the covalent bonds are formed especially in the Zn^{2+} substitution case. In this subsection, the thermodynamic stability of the substitutional defects is evaluated, and the difference between HAp and OCP as well as the site dependence is investigated.

Figure 9 shows the formation energies of substitutional Mg^{2+} and Zn^{2+} in HAp and OCP as a function of pH. Here, the energies are obtained by assuming the chemical equilibrium with the HAp-saturated solution in which the Mg^{2+} or Zn^{2+} concentration is set at 1.0×10^{-3} mol/l as found in physicological conditions.

As a general trend, it can be seen that the formation energies tend to increase with decreasing pH. This tendency

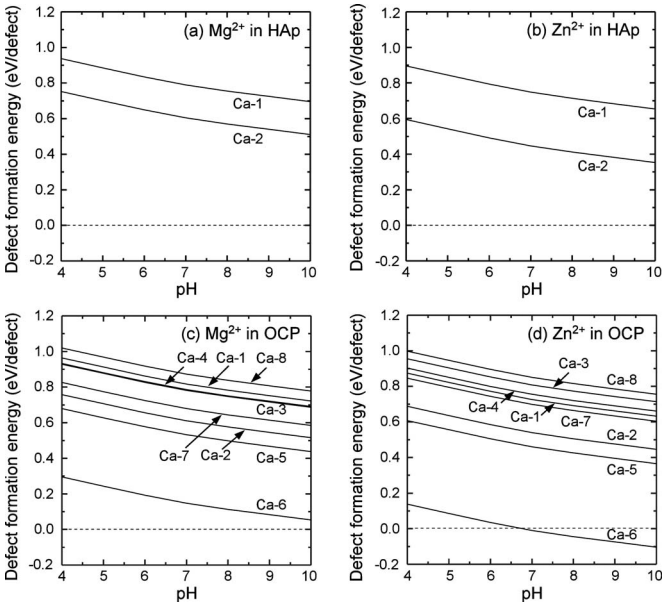

FIG. 9. Defect formation energies of substitutional Mg^{2+} and Zn^{2+} in HAp and OCP as a function of pH. In this case, the results are obtained by assuming the ionic concentrations of Mg^{2+} and Zn^{2+} in the solution to be 1.0×10^{-3} mol/l.

is attributed to variations of chemical potentials for Ca^{2+} in Eq. (1) against the solution pH. As can be seen in Fig. 2, the Ca^{2+} concentration (activity) in the solution increases with lowering pH. In such a low pH range, Ca^{2+} release from HAp or OCP into the solution by exchange with M^{2+} is difficult to occur, which results in the increase in formation energies of the substitutional defects with smaller pH.

For Mg^{2+} and Zn^{2+} in HAp [Figs. 9(a) and 9(b)], it is found that the formation energies for substitutional Zn^{2+} are smaller than those of the Mg^{2+} case. This tendency is consistent with the experimental trend reported by Suzuki *et al.* showing the much larger ion-exchange ability for Zn^{2+} in HAp than for Mg^{2+}.[32] As stated in Fig. 6, Zn^{2+} is more covalently bonded to the surrounding oxygen in HAp, which is thought to be the main reason of the relative stability of the two substitutional cations. Moreover, in both the Mg^{2+} and Zn^{2+} cases, the replacement at the Ca-2 site is energetically more favorable than that at the Ca-1 site. Regarding the site preference of different-sized foreign cations substituting for the two Ca sites in HAp, Elliot discussed a spatial difference between the two Ca sites in the original HAp lattice. If the coordination numbers of the Ca sites within the second NN coordination shell of perfect HAp are considered,[25] the Ca-1 site is in the ninefold coordination with oxygen, whereas the Ca-2 site has the sevenfold coordination. In general, larger-sized cations tend to have a larger coordination number with the surrounding anions to form more ionic bonds, while smaller-sized cations prefer to occupy smaller coordination sites so as to reduce electrostatic repulsion between the surrounding anions. Also, the average Ca–O length for Ca-1 of 0.257 nm is larger than that for Ca-2 (0.247 nm). Based on this simple geometrical consideration, it is expected that the smaller-sized Mg^{2+} and Zn^{2+} prefer to occupy the Ca-2 site in HAp. It is noted that the preference of the Ca-2 site for Zn^{2+} substitution in HAp is consistent with the first-principles result by Ma and Ellis, although they treated the substitution on the HAp (0001) surface.[19]

When Mg^{2+} and Zn^{2+} are incorporated in OCP [Figs. 9(c) and 9(d)], they have the formation energies at most of the Ca sites similar to those in HAp. It can be seen, however, that the formation energies at the Ca-6 site become considerably small for both Mg^{2+} and Zn^{2+}, as compared to those at the other Ca sites. This can also be explained by the geometrical consideration for the Ca sites in OCP. As also stated in the HAp case, since Mg^{2+} and Zn^{2+} are much smaller in size than Ca^{2+}, it is expected that they can easily occupy the Ca sites having the smaller coordination numbers with oxygen. As can be seen in Table I, the lower coordinated Ca sites (sixfold) in the original OCP lattice correspond to Ca-3, Ca-5, Ca-6, and Ca-8. Among them, the average bond length of Ca–O at the Ca-6 site is the smallest (0.240 nm), which indicates that Ca-6 is a plausible substitutional site for small-sized Mg^{2+} and Zn^{2+}. It is noted that the Ca-5 site is also sixfold coordinated by oxygen with the average bond length of 0.241 nm, which is quite similar to Ca-6. In fact, it is found in Fig. 9 that the substitution at the Ca-5 site also shows the relatively smaller formation energies than the other substitution cases except for Ca-6.

It is also worth mentioning here that Zn^{2+} at Ca-6 exhibits the smaller formation energy than Mg^{2+} at Ca-6. The formation energy of Zn^{2+} at Ca-6 becomes negative above neutral pH. It can be said that Zn^{2+} can completely replace Ca^{2+} ions at the Ca-6 site of OCP in the neutral and alkaline aqueous conditions.

Based on the calculated formation energies of substitutional Mg^{2+} and Zn^{2+} in HAp and OCP, their equilibrium concentrations $C_{M^{2+}}$ are evaluated. Then, the following equation is employed:

$$C_{M^{2+}} = \exp\left(-\frac{\Delta H_f}{k_B T}\right). \tag{12}$$

As shown in Fig. 9, the formation energies strongly depend on the substitutional sites. Therefore, the site occupancies of the substitutional ions are individually calculated for all the Ca sites in HAp and OCP, and are summed up to evaluate the concentrations of substitutional Mg^{2+} and Zn^{2+} in the respective crystals.

Figure 10 displays the equilibrium concentrations of Mg^{2+} and Zn^{2+} in HAp and OCP against pH of the surrounding solution (at 298 K). Since the defect formation energies also depend on the ionic contents of Mg^{2+} and Zn^{2+} in the solution $[M^{2+}]$, the results for $[M^{2+}]=1.0\times10^{-4}$ mol/l are also plotted for comparison.

In this figure, it is noted that the results of Mg^{2+} and Zn^{2+} in HAp cannot be observed. This is because the evaluated defect concentrations in HAp at 298 K are less than 10^{-6} at. % due to the relatively large formation energies [see Figs. 9(a) and 9(b)]. This indicates that Mg^{2+} and Zn^{2+} substitution for Ca^{2+} is quite difficult to take place in the HAp structure.

Regarding the solubility of Mg^{2+} and Zn^{2+} in HAp, contradictory data were experimentally reported. Pantel indicated that Mg^{2+} can be incorporated in HAp to form the solid

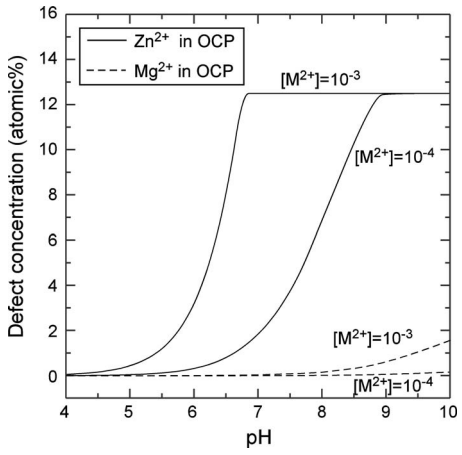

FIG. 10. Equilibrium concentrations of the substitutional defects as a function of pH. Here only the results for OCP can be observed because of the much smaller defect concentrations in HAp.

solution,[40] whereas Neuman and Muhyan[41] and Bigi *et al.*[6] showed that most of Mg^{2+} ions in the HAp-solution system cannot be incorporated inside HAp crystals and are limited to be loosely bound at HAp surfaces. LeGeros also suggested a quite limited replacement of Ca^{2+} by Mg^{2+} in HAp.[42] More recently, Kannan *et al.* reported magnesium incorporation in mixtures of HAp and β-TCP but there is no indication of Mg^{2+} substitution in the HAp lattice.[43] Likewise, formation of zinc-calcium HAp solid solution was also reported,[44] and yet Bigi *et al.*[7] later indicated the difficulty of Zn^{2+} incorporation into HAp. Miyaji *et al.* showed that the substituting limit of Zn in synthetic HAp is about 15 mol %.[45] In this regard, the present results show the extreme difficulty of Mg^{2+} and Zn^{2+} incorporation in HAp. In addition, it is known that Mg^{2+} and Zn^{2+} added in the aqueous solution inhibit HAp crystallization and destabilize the HAp crystalline phase.[6,7] This may also imply that the incorporation of Mg^{2+} and Zn^{2+} in HAp is essentially not energetically favorable.

In contrast, it can be seen that OCP can accept much more substitutional Mg^{2+} and Zn^{2+}, depending on the surrounding pH condition, and that Zn^{2+} is more incorporated in OCP, as compared to Mg^{2+}. The substitutional Zn^{2+} concentration in OCP readily increases with increasing pH. In the case of $[M^{2+}]=1.0\times10^{-3}$ mol/l, $C_{Zn^{2+}}$ is saturated at 12.5 at. %, which corresponds to the fully substituted Ca-6 site by Zn^{2+} in OCP. In fact, it is observed in Fig. 9 that the formation energy of Zn^{2+} at Ca-6 becomes zero at around neutral pH. Since the formation energies at the other Ca sites exhibit larger values than that at Ca-6, the Zn^{2+} concentrations at the Ca sites except for Ca-6 are actually negligible. In contrast, the Mg^{2+} concentration in OCP around neutral pH is much smaller than the Zn^{2+} case, which can be understood from the larger formation energy of Mg^{2+} at Ca-6 shown in Fig. 9(c).

Based on the present results, it can be said that the biological effects of Mg^{2+} and Zn^{2+} to enhance bone formation cannot be directly related to their incorporation into HAp crystals. Since Zn^{2+} can be easily incorporated in OCP by exchange with Ca^{2+}, however, it can be expected that Zn^{2+} play its biological role by being located at the low-crystalline transition region on HAp crystals. In this case, it may be speculated that Zn^{2+} directly promotes adsorption and activity of osteoblast cells at the transition region, which may contribute to the enhanced bone formation. In contrast, Mg^{2+} is much more difficult to substitute for Ca even in OCP. Since hard tissues such as bone and tooth is a mixture of apatite minerals and organic components of collagen and water, most of Mg^{2+} may be located in the organic part or in the surrounding body fluid. If this is the case, Mg^{2+} ions are readily available to directly act on cells and enzyme to promote bone formation.[13]

It is finally noted that the present study dealt with the single substitution of Mg^{2+} and Zn^{2+} for Ca^{2+} in the perfect lattices of HAp and OCP. As a matter of fact, biological HAp also contains a certain amount of other foreign cations and anions, and, in particular, the carbonate (CO_3^{2-}) content is much larger than those of all the other impurities,[1] which will affect the solubility of other trace elements. In this regard, Tas reported that, when HAp powders are precipitated in simulated body fluid (SBF) solution, Mg^{2+} and CO_3^{2-} ions coming from the SBF are favorably incorporated in the powders.[46] This is an indication of cosubstitution of the ions in HAp, which should be further addressed in future.

IV. CONCLUSIONS

In this study, first-principles calculations are performed for Mg^{2+} and Zn^{2+} substitution in HAp and OCP, in order to reveal their possible location in the system of HAp in contact with the aqueous solution. OCP is assumed to be a structural model of the transition region between HAp and the solution. Owing to the smaller ionic sizes of Mg^{2+} and Zn^{2+} than Ca^{2+}, the substitution for Ca sites of HAp and OCP brings about considerable inward atomic relaxation of the surrounding oxygen ions, which results in the smaller coordination numbers with oxygen as compared with that of Ca in bulk HAp and OCP. It is also found that the substitutional Zn^{2+} ions tend to form the covalent bonds with oxygen in the fourfold coordination state.

From the calculated defect formation energies, it is likely that the substitutional foreign ions are quite difficult to dissolve into HAp whereas can be more easily incorporated in OCP. In particular, Zn^{2+} can more favorably substitute for the specific Ca site of OCP, as compared to Mg^{2+}, due to the covalent character of bonding.

ACKNOWLEDGMENTS

This study was supported by Grant-in-Aid for Scientific Research on Priority Areas "Nano Materials Science for Atomic Scale Modification 474" from Ministry of Education, Culture, Sports, Science and Technology (MEXT) of Japan. The author also acknowledges I. Tanaka for his support of computation.

[1] S. V. Dorozhkin, J. Mater. Sci. **42**, 1061 (2007).
[2] R. K. Rude, H. E. Gruber, L. Y. Wei, A. Frausto, and B. G. Mills, Calcif. Tissue Int. **72**, 32 (2003).
[3] H. Kawamura, A. Ito, S. Miyakawa, P. Layrolle, K. Ojima, N. Ichinose, and T. Tateishi, J. Biomed. Mater. Res. **50**, 184 (2000).

[4] S. Hayakawa, K. Ando, K. Tsuru, A. Osaka, E. Fujii, and K. Kawabata, J. Am. Ceram. Soc. **90**, 565 (2007).
[5] A. Bigi, E. Foresti, R. Gregorini, A. Ripamonti, N. Roveri, and J. S. Shah, Calcif. Tissue Int. **50**, 439 (1992).
[6] A. Bigi, G. Falini, E. Foresti, M. Grazzano, A. Ripamonti, and N. Roveri, J. Inorg. Biochem. **49**, 69 (1993).
[7] A. Bigi, E. Foresti, M. Gandolfi, M. Grazzano, and N. Roveri, J. Inorg. Biochem. **58**, 49 (1995).
[8] N. Kanzaki, K. Onuma, G. Treboux, S. Tsutsumi, and A. Ito, J. Phys. Chem. B **104**, 4189 (2000).
[9] W. E. Brown and L. C. Chow, Colloids Surf. **7**, 67 (1983).
[10] M. S. Tung and D. Skrtic, in *Octacalcium Phosphate*, Monograph Oral Science Vol. 18, edited by L. C. Chow and E. D. Eanes (Basel, Karger, 2001), p. 112.
[11] M. S. A. Johnsson and G. H. Nancollas, Crit. Rev. Oral Biol. Med. **3**, 61 (1992).
[12] R. A. Santos, R. A. Wind, and C. E. Bronnimann, J. Magn. Reson., Ser. B **105**, 183 (1994).
[13] S. Cazalbou, D. Eichert, X. Ranz, C. Drouet, C. Combes, M. F. Harmand, and C. Rey, J. Mater. Sci. **16**, 405 (2005).
[14] W. E. Brown, M. Mathew, and M. S. Tung, Prog. Cryst. Growth Charact. **4**, 59 (1981).
[15] K. Matsunaga and A. Kuwabara, Phys. Rev. B **75**, 014102 (2007).
[16] P. Rulis, H. Yao, L. Ouyang, and W. Y. Ching, Phys. Rev. B **76**, 245410 (2007).
[17] J. Terra, M. Jiang, and D. E. Ellis, Philos. Mag. A **82**, 2357 (2003).
[18] X. Yin, L. Calderin, M. J. Stott, and M. Sayer, Biomaterials **23**, 4155 (2002).
[19] X. Ma and D. E. Ellis, Biomaterials **29**, 257 (2008).
[20] G. Kresse and J. Furthmüller, Phys. Rev. B **54**, 11169 (1996).
[21] P. E. Blöchl, Phys. Rev. B **50**, 17953 (1994).
[22] G. Kresse and D. Joubert, Phys. Rev. B **59**, 1758 (1999).
[23] J. P. Perdew, K. Burke, and M. Ernzerhof, Phys. Rev. Lett. **77**, 3865 (1996).
[24] M. I. Kay, R. A. Young, and A. S. Posner, Nature (London) **204**, 1050 (1964).
[25] J. C. Elliot, *Structure and Chemistry of the Apatites and Other Calcium Orthophosphates* (Elsevier, Amsterdam, 1994).
[26] M. Mathew, W. E. Brown, and L. W. Schroeder, J. Crystallogr. Spectrosc. Res. **18**, 235 (1988).
[27] C. A. Beevers, Acta Crystallogr. **11**, 273 (1958).
[28] H. J. Monkhorst and J. D. Pack, Phys. Rev. B **13**, 5188 (1976).
[29] J. R. Pliego, Jr. and J. M. Riveros, Chem. Phys. Lett. **332**, 597 (2000).
[30] J. Llano and L. A. Eriksson, J. Chem. Phys. **117**, 10193 (2002).
[31] D. D. Wagman, W. H. Evans, V. B. Parker, R. H. Schumm, I. Halow, S. M. Bailey, K. L. Churney, and R. L. Nuttall, *The NBS Tables of Chemical Thermodynamic Properties*, J. Phys. Chem. Ref. Data **11**, 1 (1982).
[32] T. Suzuki, T. Hatsushika, and Y. Hayakawa, J. Chem. Soc., Faraday Trans. 1 **77**, 1059 (1981).
[33] S. Chander and D. W. Fuerstenau, J. Colloid Interface Sci. **70**, 506 (1979).
[34] R. M. H. Verbeeck, H. Steyaert, H. P. Thun, and F. Verbeek, J. Chem. Soc., Faraday Trans. 1 **76**, 209 (1980).
[35] K. Matsunaga, Phys. Rev. B **77**, 104106 (2008).
[36] L. Calderin, M. J. Stott, and A. Rubio, Phys. Rev. B **67**, 134106 (2003).
[37] P. Rulis, L. Ouyang, and W. Y. Ching, Phys. Rev. B **70**, 155104 (2004).
[38] See EPAPS Document No. E-JCPSA6-128-807824 for tables of the calculated structural data of the substitutional defects. For more information on EPAPS, see http://www.aip.org/pubservs/epaps.html.
[39] R. A. Shannon, Acta Crystallogr., Sect. A: Cryst. Phys., Diffr., Theor. Gen. Crystallogr. **32**, 751 (1976).
[40] P. N. Pantel, J. Inorg. Nucl. Chem. **42**, 1129 (1980).
[41] W. F. Neuman and B. J. Mulryan, Calcif. Tissue Res. **7**, 133 (1971).
[42] R. Z. LeGeros, in *Tooth Enamel IV*, edited by R. W. Fearnhead and S. Suga (Elsevier, Amsterdam, 1984), pp. 32–36.
[43] S. Kannan, F. Goetz-Neunhoeffer, J. Neubauer, and J. M. F. Ferreira, J. Am. Ceram. Soc. **91**, 1 (2008).
[44] N. K. Tripathy, P. N. Patel, and A. Panda, J. Solid State Chem. **80**, 1 (1989).
[45] F. Miyaji, Y. Kono, and Y. Suyama, Mater. Res. Bull. **40**, 209 (2005).
[46] A. C. Tas, Biomaterials **21**, 1429 (2000).